ACS OMEGA

http://pubs.acs.org/journal/acsodf

Article

Reaction Behavior of a Silicide Electrode with Lithium in an Ionic-Liquid Electrolyte

Yasuhiro Domi, Hiroyuki Usui, Kai Sugimoto, Kazuma Gotoh, Kei Nishikawa, and Hiroki Sakaguchi*

Cite This: *ACS Omega* 2020, 5, 22631−22636

Read Online

ACCESS | Metrics & More | Article Recommendations | Supporting Information

ABSTRACT: Silicides are attractive novel active materials for use in the negative-electrodes of next-generation lithium-ion batteries that use certain ionic-liquid electrolytes; however, the reaction mechanism of the above combination is yet to be clarified. Possible reactions at the silicide electrode are as follows: deposition and dissolution of Li metal on the electrode, lithiation and delithiation of Si, which would result from the phase separation of the silicide, and alloying and dealloying of the silicide with Li. Herein, we examined these possibilities using various analysis methods. The results revealed that the lithiation and delithiation of silicide occurred.

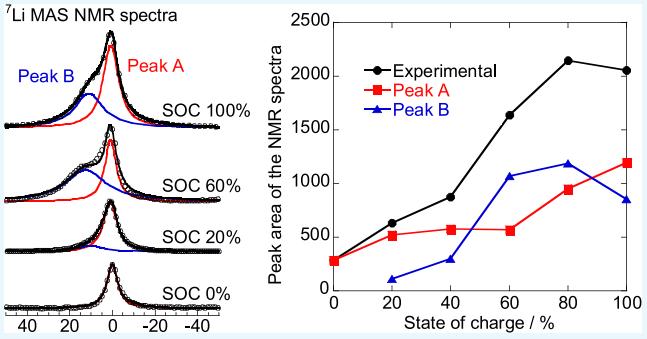

1. INTRODUCTION

The development of high-performance lithium-ion batteries (LIBs) with a high energy density, a long cycle life, and an adequate level of safety is critical to establish a sustainable society because LIBs are used as a power source in electric vehicles and as stationary batteries for utilizing renewable energy.[1,2] Silicon (Si) has great potential as an active material for negative-electrodes in next-generation LIBs due to its higher theoretical capacity (3580 mA h g^{-1} for $Li_{15}Si_4$) than that of the currently used graphite (372 mA h g^{-1} for LiC_6). However, Si electrodes show poor cycling performance, which is largely caused by a massive volume change in the Si electrode during lithiation (charge) and delithiation (discharge).[3,4] Si has additional drawbacks, namely, a low Li^+ diffusion coefficient and high electrical resistivity, thereby preventing the practical application of Si electrodes.[5,6] To solve these issues, many researchers have put in a lot of work toward the construction of new active materials including the following: synthesizing nanostructured Si materials that accommodate volume expansion,[7,8] coating of Si with conductive materials to reduce the electrical resistivity,[9,10] doping of Si with impurities including phosphorous, boron, and so on, to improve its electronic conductivity and/or change its properties, such as its phase transition, crystallinity morphology, and Li^+ diffusion,[6,11−13] preparing composites consisting of elemental Si and binary or ternary transition metal silicide to cover the shortcomings of Si,[14−17] and prelithiation of Si to decrease the relative volume change in Si during charge/discharge reactions.[18]

An electrolyte contributes toward improving the performance and safety of rechargeable batteries.[19−24] In particular, ionic liquids have superior physicochemical properties as electrolyte solvents: negligible vapor pressure, nonflammability, and a wide electrochemical window.[25−28] Silicide electrodes have shown poor cycling performance in conventional organic-liquid electrolytes.[15,16,29] In contrast, we have reported that some binary silicides can be used as novel negative-electrodes for LIBs in certain ionic-liquid electrolytes; for example, $NiSi_2$, $FeSi_2$, and Cu_3Si electrodes maintain high reversible capacity in 1 mol dm^{-3} (M) lithium bis(fluorosulfonyl)amide (LiFSA) dissolved in *N*-methyl-*N*-propylpyrrolidinium bis(fluorosulfonyl)amide (Py13-FSA).[29] Additionally, the volumetric energy density of LIBs using silicide electrodes will inevitably be high because the density of silicides (approximately 5 g cm^{-3}) is more than double that of silicon (2.33 g cm^{-3}). However, the reaction mechanism of silicide electrodes has not yet been clarified. In contrast, the lithium storage mechanism of other Si-based electrodes has been reported.[30,31]

Possible reactions at the silicide electrode are as follows: (1) deposition and dissolution of Li metal on the silicide ($Li^+ + e^- \rightarrow Li$), (2) lithiation and delithiation of Si, which would result from the phase separation of the silicide ($FeSi_2 + xLi^+ + xe^- \rightarrow Li_xSi_2 + Fe$ and/or $FeSi_2 + xLi^+ + xe^- \rightarrow Li_xSi + FeSi$), and (3) alloying and dealloying of the silicide with Li ($FeSi_2 + xLi^+ + xe^- \rightarrow Li_xFeSi_2$). In this study, we examined these possibilities using solid-state ^7Li magic-angle spinning (MAS) nuclear

Received: July 17, 2020
Accepted: August 12, 2020
Published: August 26, 2020

https://dx.doi.org/10.1021/acsomega.0c03357
ACS Omega 2020, 5, 22631−22636

magnetic resonance (NMR), X-ray diffraction (XRD), Raman spectroscopy, transmission electron microscopy (TEM), and energy-dispersive X-ray spectroscopy (EDS).

2. EXPERIMENTAL SECTION

2.1. Synthesis of Silicide Powder and Electrode Preparation. Binary silicide of $FeSi_2$ was synthesized by a mechanical alloying (MA) method. Commercially available silicon (99.9%) and iron (99.9%) powders were purchased from FUJIFILM Wako Pure Chemical Corporation, Ltd. A mixture of these powders was put in a zirconia vessel together with balls. The Si/Fe molar ratio was 3.0 and the weight ratio of the balls to the mixture was approximately 15:1. The MA was done using a high-energy planetary ball mill (P-6, Fritsch) at 380 rpm for 70 h. Although the mixture ratio was higher than the stoichiometric ratio, no elemental Si was detected in the XRD pattern and Raman spectrum. Hence, a residue on the ball and/or inside wall of the vessel should include excess Si.[29]

An $FeSi_2$ electrode was prepared by slurry coating and gas deposition (GD) methods for NMR and TEM measurements, respectively. We used acetylene black (AB), styrene−butadiene rubber (SBR), and carboxymethyl cellulose (CMC) as the conductive agent, binder, and thickener, respectively. The ratio of $FeSi_2$/AB/SBR/CMC was 70/15/5/10 wt %. Deionized water was used as a dispersing agent. The prepared slurry was coated on a Cu current collector and was dried at 120 °C to form an active material layer. The GD method requires no conductive agent or binder, and its detailed conditions have been reported in our papers.[6]

2.2. Cell Assembly and Charge and Discharge Testing. A 2032-type coin cell was assembled in an Ar-filled glovebox (Miwa MFG, DBO-2.5LNKP-TS) with a dew point below −90 °C and an oxygen content less than 1 ppm. An $FeSi_2$ electrode, a glass fiber filter (Whatman GF/A), and a Li metal sheet (thickness: 1 mm, 99.90%, Rare Metallic Co., Ltd.) were used as the working electrode, the separator, and the counter electrode, respectively. The ionic-liquid electrolyte used was 1 M LiFSA/Py13-FSA. Electrolyte preparation was also performed in the glovebox.

Galvanostatic charge−discharge testing was performed using an electrochemical measurement system (HJ-1001SM8 or HJ-1001SD8, Hokuto Denko, Co., Ltd.) in the potential range between 0.005 and 2.000 V vs Li^+/Li at 30 °C with no capacity limit. The current density was set at 50 mA g^{-1}. Then, the cell was discharged and charged to adjust the state of charge (SOC) for each point of the NMR measurement. The pre-cycling was performed by the following procedures to form a stable surface film on the $FeSi_2$ electrode: the electrode was charged from an open-circuit potential to 0.500 V vs Li^+/Li at 50 mA g^{-1}, and maintained at 0.500 V vs Li^+/Li for 12 h. Then, it was discharged from 0.500 to 2.000 V vs Li^+/Li at 50 mA g^{-1}.

2.3. Solid-State ^{7}Li MAS NMR. The coin cell was disassembled in the Ar-filled glovebox after predefined charge−discharge testing. The $FeSi_2$ slurry electrode was washed thoroughly with diethyl carbonate (DEC) before drying. The active material layer was exfoliated from a Cu current collector using a spatula to seal into a 3.2 mmϕ sample rotor for the NMR measurement. ^{7}Li MAS NMR spectra of $FeSi_2$ at each SOC were obtained using an NMR system (11.7 T magnet, DD2 Agilent Technologies Inc.) at a MAS frequency of 14 kHz. The chemical shifts were referenced to a 1 M aqueous LiCl solution. The peak fitting of NMR spectra was carried out by Origin Pro 8.5.0J (LightStone) software.

2.4. TEM Observations. After charge−discharge testing, the cell was disassembled in the glovebox, and the $FeSi_2$ GD electrode was washed with propylene carbonate and DEC before drying. We sliced the electrode into thin sections using focused ion beam scanning electron microscopy (FIB-SEM, SMF2000, Hitachi High-Tech Science Corp.) or FIB (JIB-4501, JEOL, Co., Ltd.). For the FIB process, the electrode surface was protected against damage by the Ga ion beam by carbon coating. The sliced electrode was not exposed to the atmosphere until it was introduced into the chamber of the TEM instrument (JEM-ARM200F, JEOL, Co., Ltd.) using a transfer vessel. TEM observation was performed at 200 kV and energy-dispersive X-ray spectroscopy (EDS) was performed with 10 scans.

3. RESULTS AND DISCUSSION

3.1. Possibility of the Deposition and Dissolution of Li Metal on the Silicide. Figure 1a shows the second charge−discharge curves of the $FeSi_2$ slurry and GD electrodes in 1 M LiFSA/Py13-FSA. Herein, we displayed the second curves because the first charge profile included the reductive decomposition reaction of the electrolyte. The charge−discharge profile of the slurry electrode is similar to that of the GD electrode and hence, other contents, such as AB, SBR,

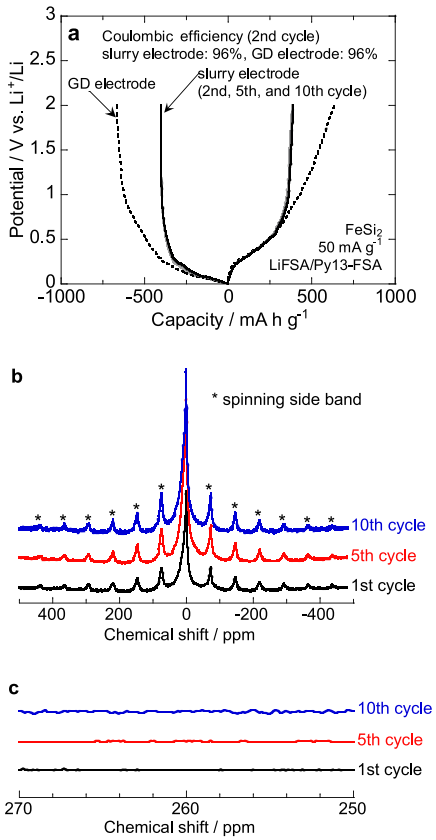

Figure 1. (a) Second charge−discharge curves of $FeSi_2$ slurry and GD electrodes in 1 M LiFSA/Py13-FSA at 50 mA g^{-1}. For comparison, the 5th and 10th curves of the slurry electrode are also shown. (b) ^{7}Li MAS NMR spectra of fully lithiated $FeSi_2$ slurry electrodes during each cycle in 1 M LiFSA/Py13-FSA at 50 mA g^{-1} and (c) their magnified view.

https://dx.doi.org/10.1021/acsomega.0c03357
ACS Omega 2020, 5, 22631−22636

and CMC in the slurry electrode, did not contribute to the electrochemical activity. Additionally, it was confirmed that the charge−discharge reaction of the $FeSi_2$ slurry electrode was stable because the 5th and 10th curves were almost the same as the second curve.

Figure 1b shows the ^{7}Li MAS NMR spectra of the $FeSi_2$ electrodes in a fully lithiated state during each cycle in the ionic-liquid electrolyte (1 M LiFSA/Py13-FSA). No peak arising from Li metal appeared at approximately 260 ppm (Figure 1c),[32] whereas we could confirm a main peak at approximately 0 ppm (discussed below) and some spinning sidebands. Consequently, we concluded that no deposition or dissolution of Li metal occurred on the silicide electrode.

3.2. Possibility of Phase Separation of $FeSi_2$. To clarify whether the phase separation of $FeSi_2$ into Si and Fe and/or Si-poor Fe−Si phases occurs ($FeSi_2 + xLi^+ + xe^- \rightarrow Li_xSi_2 + Fe$ and/or $FeSi_2 + xLi^+ + xe^- \rightarrow Li_xSi + FeSi$), we investigated the phase transition of the $FeSi_2$ electrode during charge−discharge cycling. Figure 2 provides the XRD pattern of the

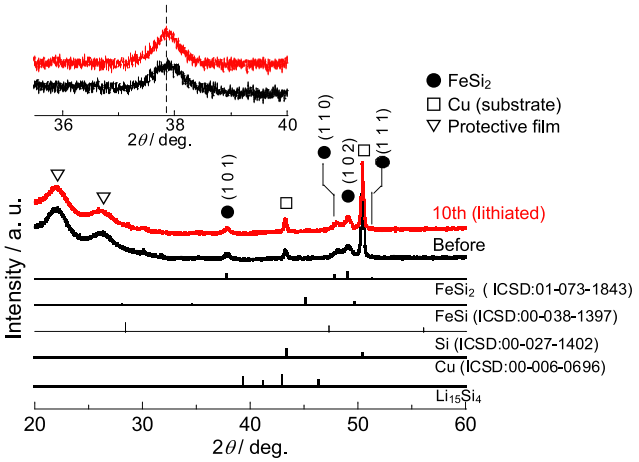

Figure 2. XRD pattern of the fully lithiated $FeSi_2$ electrode during the 10th cycle in 1 M LiFSA/Py13-FSA at 50 mA g^{-1} and its magnified view. The XRD pattern before cycling is also shown.

fully lithiated $FeSi_2$ electrode during the 10th cycle. The pattern showed no new peaks that would represent Si, Fe, FeSi, and $Li_{15}Si_4$ phases.[33] In fact, all peaks looked the same as those assigned to the $FeSi_2$ phase before cycling; additionally, these peaks did not shift, as shown in the inset. The results revealed that $FeSi_2$ maintains its crystal structure before and after charge−discharge cycling. Additionally, we have previously confirmed that no peaks assigned to crystalline and/or amorphous Si appear in the Raman spectra of $FeSi_2$ after cycling.[29] However, if the phase separation occurs at an extreme surface of the $FeSi_2$ electrode and ultrafine particles (100 nm or less) of Si form, the particles will not be detected due to the finite resolution of the Raman spectrometer. Thus, we observed a cross section of the $FeSi_2$ electrode after charge−discharge testing by TEM.

Figure 3 displays the bright-field (BF) TEM images of the $FeSi_2$ electrode after the fifth cycle and the corresponding EDS mappings of Fe and Si. The active material layer consisted of Fe and Si, as shown in Figure 3a−c, and these elements are also evenly distributed in the enlarged views (Figure 3d−i). To confirm whether the observed active material layer is $FeSi_2$ and includes Si that results from phase separation, we measured a selected area electron diffraction (SAED) pattern at area III in Figure 3a (Figure S1), and the obtained *d*-spacings are summarized in Table S1. Because all *d*-spacings were assigned to $FeSi_2$, the active material layer was still $FeSi_2$ after cycling. The XRD, Raman, and TEM results demonstrated that no phase separation of $FeSi_2$ into Si and Fe and/or Si-poor Fe−Si phases occurred and hence, the reversible capacity of the $FeSi_2$ electrode did not result from the lithiation and delithiation reactions of Si.

3.3. Verification of the Alloying and Dealloying of the Silicide with Li. Finally, we expected that $FeSi_2$ itself reacts with Li. Figure 4a shows the ^{7}Li MAS NMR spectra of the $FeSi_2$ electrodes at various state of charge (SOC) values during the fifth cycle in the ionic-liquid electrolyte. At a high SOC, a shoulder at approximately 11 ppm appeared in addition to a main peak at approximately 0 ppm. Based on the deconvolution of the peak, we defined the peaks at 0 and 11 ppm as Peak A and Peak B, respectively. The appearance of two peaks indicated two possibilities: (a) Li existed in two different chemical environments in the same matter, that is, $FeSi_2$, or (b) Li reacted with two different substances (e.g., Si and FeSi). Although Peak A only appeared at an SOC of 0%, Li should not be stored in $FeSi_2$ because the electrode potential would be too high (Figure S2); thus, Peak A at an SOC of 0% should be assigned to Li in the surface film formed on the $FeSi_2$ electrode through the reductive decomposition of the electrolyte or the Li salt in the electrolyte (LiFSA). Extremely sharp NMR spectra of LiFSA appeared at approximately −1 ppm and we washed the electrode thoroughly with DEC. Additionally, it has been reported that Li-containing compounds, such as Li_2O, Li_2CO_3, in the surface film on the electrode exhibited an NMR peak at approximately 0 ppm.[34−36] Therefore, we concluded that Peak A at an SOC of 0% could be attributed to Li in the surface film.

The intensity of Peaks A and B increased with an increase in the SOC (20−100%), whereas their peak position was approximately constant, as shown in Figure 4b,c. Because the fifth Coulombic efficiency was 98.2% (Figure S3), it was unlikely that the growth of the surface film caused an increase in Peak A. Key et al.[37,38] reported ex situ ^{7}Li NMR spectra of Si, namely, $Li_{12}Si_7$ and $Li_{15}Si_4$ phases exhibit peaks at 18.0 and 6.0 ppm, which are assigned to Li surrounding small Si clusters and Li near isolated Si, respectively. The peak centered at 18.0 ppm shifts toward a higher magnetic field (lower chemical shift) with a decrease in cluster size (planar Si_5 rings, trigonal−planar Si_4 clusters, and Si−Si dumbbells), thereby forming Li_7Si_3 and/or $Li_{13}Si_4$ phases. Additionally, a peak arising from overlithiated Si ($Li_{15+\delta}Si_4$) phases appeared with a negative chemical shift.[37] The chemical shift of Peak A did not correspond to the above Li−Si alloy phases; therefore, Peak A between an SOC of 20 and 100% is attributed to Li stored in $FeSi_2$.

There remains a possibility that Peak B could be assigned to the $Li_{13}Si_4$ phase because the Li−Si alloy showed an NMR peak at approximately 11.5 ppm. However, the results of Figures 2 and 3 showed no presence of Si during charge−discharge testing; thus, Peak B would arise from Li stored in the different chemical environments of $FeSi_2$. Therefore, the NMR results revealed the existence of two different chemical environments for Li storage in $FeSi_2$, thereby showing that the lithiation and delithiation of the $FeSi_2$ electrode occurred ($FeSi_2 + xLi^+ + xe^- \rightarrow Li_xFeSi_2$). We consider that the reaction occurs not only in the ionic-liquid electrolyte but also in the organic-liquid electrolyte.[29]

https://dx.doi.org/10.1021/acsomega.0c03357
ACS Omega 2020, 5, 22631−22636

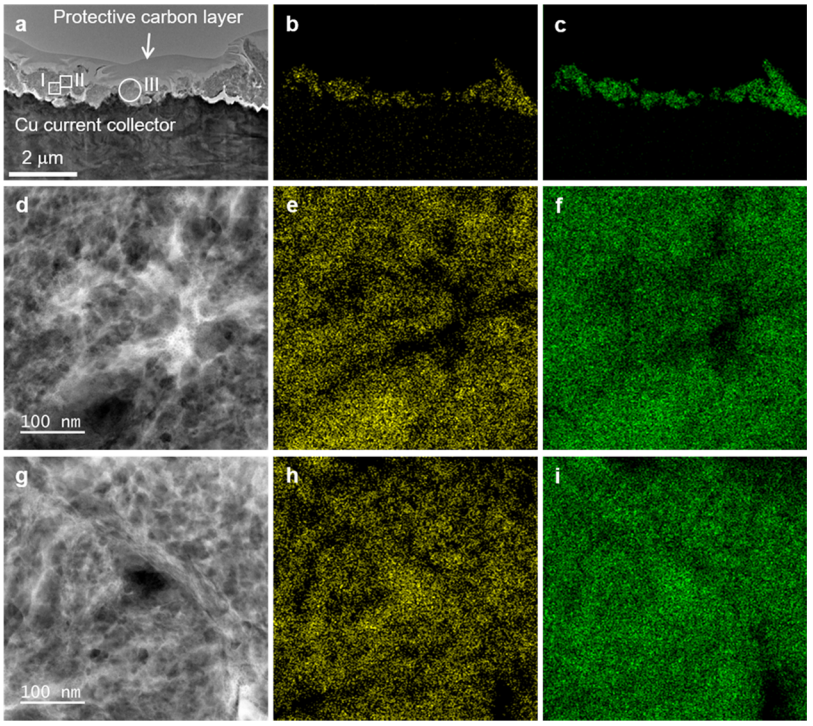

Figure 3. (a) BF-TEM image of the $FeSi_2$ electrode after the fifth cycle in 1 M LiFSA/Py13-FSA at 50 mA g^{-1} and the corresponding EDS mappings of (b) Fe and (c) Si. The (d–f) and (g–i) images correspond to areas I and II in part (a), respectively, and area III denotes the SAED measurement point.

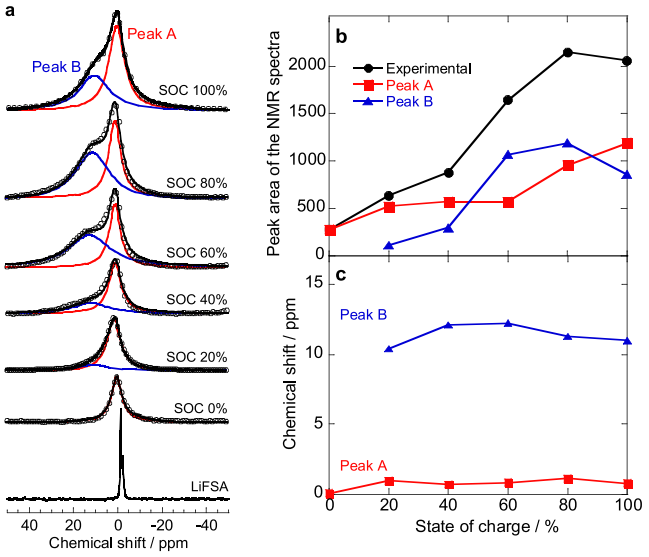

Figure 4. (a) ^{7}Li MAS NMR spectra of $FeSi_2$ from an SOC of 0–100% during the fifth cycle in 1 M LiFSA/Py13-FSA at 50 mA g^{-1} and the correlation between the SOC and (b) the peak area or (c) chemical shift.

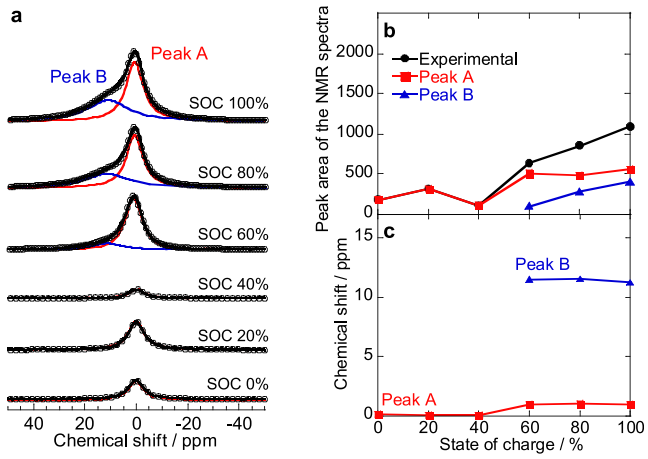

Figure 5. (a) ^{7}Li MAS NMR spectra of $FeSi_2$ from an SOC of 0–100% during the first cycle after pre-cycling in 1 M LiFSA/Py13-FSA at 50 mA g^{-1} and the correlation between the SOC and (b) the peak area or (c) chemical shift.

Because the lithiation of a crystalline or amorphous Si phase exhibited different NMR spectra,[32] we confirmed the ^{7}Li MAS NMR spectra of the $FeSi_2$ electrodes at various SOC values during the first cycle (Figure 5). To form the surface film on the electrode at an SOC of 0%, we performed pre-cycling (Figure S4). The appearance and position of Peaks A and B were almost the same as those during the fifth cycle (Figure 4), which indicated that $FeSi_2$ maintained its crystallinity, as confirmed in Figure 2; thus, no amorphous $FeSi_2$ phase was formed.

Although the lithiation and delithiation reactions of the silicide occurred among the possible reactions at the electrode, it is interesting that no peak shifts resulted in the XRD pattern (Figure 2). For instance, if Li_xFeSi_2 formed, it would be expected that the lattice constant of Li_xFeSi_2 becomes larger than that of $FeSi_2$. These results indicate that the bulk of $FeSi_2$ did not participate in the lithiation, and rather its surface was involved in alloying with Li. Therefore, the reaction sites (Peaks A and B in the NMR spectra) and reaction areas (bulk or surface) of the silicide are under further study.

https://dx.doi.org/10.1021/acsomega.0c03357
ACS Omega 2020, 5, 22631–22636

4. CONCLUSIONS

We investigated the reaction behavior of a silicide with Li in an ionic-liquid electrolyte. The XRD, Raman, and TEM results revealed that no phase separation of $FeSi_2$ into Si and Fe and/or Si-poor Fe−Si phases occurred during charge−discharge cycling; thus, the reversible capacity of the $FeSi_2$ electrode did not result from the lithiation and delithiation reactions of Si. The NMR results demonstrated that no Li metal was deposited or dissolved on the $FeSi_2$ electrode but that the lithiation and delithiation of $FeSi_2$ did occur. Additionally, there were two different chemical environments for Li storage in $FeSi_2$. Although the reaction sites (Peaks A and B in the NMR spectra) and reaction areas (bulk or surface) are still unclear, our results provide critical insights into the reaction mechanism of novel alloy-based negative electrodes for LIBs.

■ ASSOCIATED CONTENT

Supporting Information

The Supporting Information is available free of charge at https://pubs.acs.org/doi/10.1021/acsomega.0c03357.

SAED pattern; *d*-spacings; charge−discharge curves; and Coulombic efficiency values (PDF)

■ AUTHOR INFORMATION

Corresponding Author

Hiroki Sakaguchi − *Department of Chemistry and Biotechnology, Graduate School of Engineering and Center for Research on Green Sustainable Chemistry, Tottori University, Tottori 680-8552, Japan;* orcid.org/0000-0002-4125-7182; Phone: +81-857-31-5265; Email: sakaguch@tottori-u.ac.jp

Authors

Yasuhiro Domi − *Department of Chemistry and Biotechnology, Graduate School of Engineering and Center for Research on Green Sustainable Chemistry, Tottori University, Tottori 680-8552, Japan;* orcid.org/0000-0003-3983-2202

Hiroyuki Usui − *Department of Chemistry and Biotechnology, Graduate School of Engineering and Center for Research on Green Sustainable Chemistry, Tottori University, Tottori 680-8552, Japan;* orcid.org/0000-0002-1156-0340

Kai Sugimoto − *Course of Chemistry and Biotechnology, Department of Engineering, Graduate School of Sustainability Science and Center for Research on Green Sustainable Chemistry, Tottori University, Tottori 680-8552, Japan*

Kazuma Gotoh − *Graduate School of Natural Science & Technology, Okayama University, Okayama 700-8530, Japan; Element Strategy Initiative for Catalysis and Batteries (ESICB), Kyoto University, Kyoto 615-8245, Japan;* orcid.org/0000-0002-8197-5701

Kei Nishikawa − *International Center of Young Scientists, National Institute for Materials Science, Tsukuba 305-0044, Japan;* orcid.org/0000-0002-7718-7606

Complete contact information is available at: https://pubs.acs.org/10.1021/acsomega.0c03357

Author Contributions

This manuscript was written through the contributions of all authors.

Notes

The authors declare no competing financial interest.

■ ACKNOWLEDGMENTS

This work was partially supported by the Japan Society for the Promotion of Science (JSPS) KAKENHI (Grant numbers JP19K05649, JP19H02817, JP20H00399, JP17K06017, and JP18K04965) and the NIMS Joint Research Hub Program. The authors thank K. Shinoda for his assistance with the TEM observations.

■ REFERENCES

(1) Whittingham, M. S. Lithium Batteries and Cathode Materials. *Chem. Rev.* **2004**, *104*, 4271−4302.

(2) Armand, M.; Tarascon, J. M. Building Better Batteries. *Nature* **2008**, *451*, 652−657.

(3) Obrovac, M. N.; Krause, L. J. Reversible Cycling of Crystalline Silicon Powder. *J. Electrochem. Soc.* **2007**, *154*, A103−A108.

(4) Liu, X. H.; Zhong, L.; Huang, S.; Mao, S. X.; Zhu, T.; Huang, J. Y. Size-Dependent Fracture of Silicon Nanoparticles During Lithiation. *ACS Nano* **2012**, *6*, 1522−1531.

(5) Ding, N.; Xu, J.; Yao, Y. X.; Wegner, G.; Fang, X.; Chen, C. H.; Lieberwirth, I. Determination of the Diffusion Coefficient of Lithium Ions in Nano-Si. *Solid State Ionics* **2009**, *180*, 222−225.

(6) Domi, Y.; Usui, H.; Yamaguchi, K.; Yodoya, S.; Sakaguchi, H. Silicon-Based Anodes with Long Cycle Life for Lithium-Ion Batteries Achieved by Significant Suppression of Their Volume Expansion in Ionic-Liquid Electrolyte. *ACS Appl. Mater. Interfaces* **2019**, *11*, 2950−2960.

(7) Liu, B.; Wang, X.; Chen, H.; Wang, Z.; Chen, D.; Cheng, Y.-B.; Zhou, C.; Shen, G. Hierarchical Silicon Nanowires-Carbon Textiles Matrix as a Binder-Free Anode for High-Performance Advanced Lithium-Ion Batteries. *Sci. Rep.* **2013**, *3*, No. 1622.

(8) Zhou, X.; Wan, L.-J.; Guo, Y.-G. Electrospun Silicon Nanoparticle/Porous Carbon Hybrid Nanofibers for Lithium-Ion Batteries. *Small* **2013**, *9*, 2684−2688.

(9) Zhou, X.; Yin, Y.-X.; Cao, A.-M.; Wan, L.-J.; Guo, Y.-G. Efficient 3D Conducting Networks Built by Graphene Sheets and Carbon Nanoparticles for High-Performance Silicon Anode. *ACS Appl. Mater. Interfaces* **2012**, *4*, 2824−2828.

(10) Jo, C.; Groombridge, A. S.; Verpilliere, J. D. L.; Lee, J. T.; Son, Y.; Liang, H.-L.; Boies, A. M.; Volder, M. D. Continuous-Flow Synthesis of Carbon-Coated Silicon/Iron Silicide Secondary Particles for Li-Ion Batteries. *ACS Nano* **2020**, *14*, 698−707.

(11) Long, B. R.; Chan, M. K. Y.; Greeley, J. P.; Gewirth, A. A. Dopant Modulated Li Insertion in Si for Battery Anodes: Theory and Experiment. *J. Phys. Chem. C* **2011**, *115*, 18916−18921.

(12) Yi, R.; Zai, J.; Dai, F.; Gordin, M. L.; Wang, D. Improved Rate Capability of Si−C Composite Anodes by Boron Doping for Lithium-Ion Batteries. *Electrochem. Commun.* **2013**, *36*, 29−32.

(13) Domi, Y.; Usui, H.; Shimizu, M.; Kakimoto, Y.; Sakaguchi, H. Effect of Phosphorus-Doping on Electrochemical Performance of Silicon Negative Electrodes in Lithium-Ion Batteries. *ACS Appl. Mater. Interfaces* **2016**, *8*, 7125−7132.

(14) Usui, H.; Maebara, K.; Nakai, K.; Sakaguchi, H. Anode Properties of Composite Thick-Film Electrodes Consisted of Si and Various Metal Silicides. *Int. J. Electrochem. Sci.* **2011**, *6*, 2246−2254.

(15) Usui, H.; Nouno, K.; Takemoto, Y.; Nakada, K.; Ishii, A.; Sakaguchi, H. Influence of Mechanical Grinding on Lithium Insertion and Extraction Properties of Iron Silicide/Silicon Composites. *J. Power Sources* **2014**, *268*, 848−852.

(16) Domi, Y.; Usui, H.; Takemoto, Y.; Yamaguchi, K.; Sakaguchi, H. Improved Electrochemical Performance of Lanthanum Silicide/Silicon Composite Electrode with Nickel Substitution for Lithium-Ion Batteries. *J. Phys. Chem. C* **2016**, *120*, 16333−16339.

(17) Domi, Y.; Usui, H.; Takemoto, Y.; Yamaguchi, K.; Sakaguchi, H. Improved Electrochemical Performance of a Ge_xSi_{1-x} Alloy Negative Electrode for Lithium-Ion Batteries. *Chem. Lett.* **2016**, *45*, 1198−1200.

(18) Domi, Y.; Usui, H.; Iwanari, D.; Sakaguchi, H. Effect of Mechanical Pre-Lithiation on Electrochemical Performance of Silicon

Negative Electrode for Lithium-Ion Batteries. *J. Electrochem. Soc.* **2017**, *164*, A1651−A1654.
(19) Wang, J.; Yamada, Y.; Sodeyama, K.; Chiang, C. H.; Tateyama, Y.; Yamada, A. Superconcentrated Electrolytes for a High-Voltage Lithium-Ion Battery. *Nat. Commun.* **2016**, *7*, No. 12032.
(20) Matsumoto, K.; Hwang, J.; Kaushik, S.; Chen, C.-Y.; Hagiwara, R. Advances in Sodium Secondary Batteries Utilizing Ionic Liquid Electrolytes. *Energy Environ. Sci.* **2019**, *12*, 3247−3287.
(21) Yamaguchi, K.; Domi, Y.; Usui, H.; Shimizu, M.; Morishita, S.; Yodoya, S.; Sakata, T.; Sakaguchi, H. Effect of Film-Forming Additive in Ionic Liquid Electrolyte on Electrochemical Performance of Si Negative-Electrode for LIBs. *J. Electrochem. Soc.* **2019**, *166*, A268−A276.
(22) Domi, Y.; Usui, H.; Nakabayashi, E.; Yamamoto, T.; Nohira, T.; Sakaguchi, H. Potassiation and Depotassioation Properties of Sn_4P_3 Electrode in an Ionic-Liquid Electrolyte. *Electrochemistry* **2019**, *87*, 333−335.
(23) Yamamoto, T.; Nohira, T. Tin Negative Electrodes Using an FSA-Based Ionic Liquid Electrolyte: Improved Performance of Potassium Secondary Batteries. *Chem. Commun.* **2020**, *56*, 2538−2541.
(24) Qi, H.; Ren, Y.; Guo, S.; Wang, Y.; Li, S.; Hu, Y.; Yan, F. High-Voltage Resistant Ionic Liquids for Lithium-Ion Batteries. *ACS Appl. Mater. Interfaces* **2020**, *12*, 591−600.
(25) Earle, M. J.; Esperança, J. M. S. S.; Gilea, M. A.; Lopes, J. N. C.; Rebelo, L. P. N.; Magee, J. W.; Seddon, K. R.; Widegren, J. A. The Distillation and Volatility of Ionic Liquids. *Nature* **2006**, *439*, 831−834.
(26) Hapiot, P.; Lagrost, C. Electrochemical Reactivity in Room-Temperature Ionic Liquids. *Chem. Rev.* **2008**, *108*, 2238−2264.
(27) Sippel, P.; Lunkenheimer, P.; Krohns, S.; Thoms, R.; Loidl, A. Importance of Liquid Fragility for Energy Applications of Ionic Liquids. *Sci. Rep.* **2015**, *5*, No. 13922.
(28) Ghoufi, A.; Szymcxyk, A.; Malfreyt, P. Ultrafast diffusion of Ionic Liquids Confined in Carbon Nanotubes. *Sci. Rep.* **2016**, *6*, No. 28518.
(29) Domi, Y.; Usui, H.; Takaishi, R.; Sakaguchi, H. Lithiation and Delithiation Reactions of Binary Silicide Electrodes in an Ionic Liquid Electrolyte as Novel Anodes for Lithium-Ion Batteries. *ChemElectroChem* **2019**, *6*, 581−589.
(30) Zhu, G.; Zhang, F.; Li, X.; Luo, W.; Li, L.; Zhang, H.; Wang, L.; Wang, Y.; Jiang, W.; Liu, H. K.; Dou, S. X.; Yang, J. Engineering the Distribution of Carbon in Silicon Oxide Nanospheres at the Atomic Level for Highly Stable Anodes. *Angew. Chem., Int. Ed.* **2019**, *58*, 6669−6673.
(31) Yang, J.; Wang, Y.; Li, W.; Wang, L.; Fan, Y.; Jiang, W.; Luo, W.; Wang, Y.; Kong, B.; Selomulya, C.; Liu, H. K.; Dou, S. X.; Zhao, D. Amorphous TiO2 Shells: A Vital Elastic Buffering Layer on Silicon Nanoparticles for High-Performance and Safe Lithium Storage. *Adv. Mater.* **2019**, *29*, No. 1700523.
(32) Pecher, O.; Carretero-González, J.; Griffith, K. J.; Grey, C. P. Materials' Methods: NMR in Battery Research. *Chem. Mater.* **2017**, *29*, 213−242.
(33) Hatchard, T. D.; Dahn, J. R. In Situ XRD and Electrochemical Study of the Reaction of Lithium with Amorphous Silicon. *J. Electrochem. Soc.* **2004**, *151*, A838−A842.
(34) Meyer, B. M.; Leifer, N.; Sakamoto, S.; Greenbaum, S. G.; Grey, C. P. High Field Multinuclear NMR Investigation of the SEI Layer in Lithium Rechargeable Batteries. *Electrochem. Solid-State Lett.* **2005**, *8*, A145−A148.
(35) Piper, D. M.; Evans, T.; Leung, K.; Watkins, T.; Olson, J.; Kim, S. C.; Han, S. S.; Bhat, V.; Oh, K. H.; Buttry, D. A.; Lee, S. H. Stable Silicon-Ionic Liquid Interface for Next-Generation Lithium-Ion Batteries. *Nat. Commun.* **2015**, *6*, No. 6230.
(36) Budi, A.; Basile, A.; Opletal, G.; Hollenkamp, A. F.; Best, A. S.; Rees, R. J.; Bhatt, A. I.; O'Mullane, A. P.; Russo, S. P. Study of the Initial Stage of Solid Electrolyte Interphase Formation upon Chemical Reaction of Lithium Metal and N-Methyl-N-Propyl-Pyrrolidinium-Bis(Fluorosulfonyl)Imide. *J. Phys. Chem. C* **2012**, *116*, 19789−19797.
(37) Key, B.; Bhattacharyya, R.; Morcrette, M.; Seznéc, V.; Tarascon, J.-M.; Grey, C. P. Real-Time NMR Investigations of Structural Changes in Silicon Electrodes for Lithium-Ion Batteries. *J. Am. Chem. Soc.* **2009**, *131*, 9239−9249.
(38) Key, B.; Morcrette, M.; Tarascon, J.-M.; Grey, C. P. Pair Distribution Function Analysis and Solid State NMR Studies of Silicon Electrodes for Lithium Ion Batteries: Understanding the (De)lithiation Mechanisms. *J. Am. Chem. Soc.* **2011**, *133*, 503−512.

https://dx.doi.org/10.1021/acsomega.0c03357
ACS Omega 2020, 5, 22631−22636